

ARTICLE

Open Access

Transparent vertical nanotube electrode arrays on graphene for cellular recording and optical imaging

Jamin Lee^{1,2}, Keundong Lee³, Kyumeen Kang^{1,2}, Asad Ali², Dong Wook Kim², Hyerim Ahn⁴, Gwanho Ko^{5,6}, Myunghwan Choi^{5,6}, Youngbin Tchoe⁷, Hye Yoon Park⁴ and Gyu-Chul Yi^{1,2}

Abstract

Here, we report the fabrication of transparent multichannel vertical nanotube electrode arrays for detecting cellular activity and optically imaging neuronal networks. To fabricate these transparent electrode arrays, position- and morphology-controlled ZnO nanotube arrays consisting of ultrathin nanowalls were grown on transparent graphene layers and coated with Ti/Au metal layers. Using these multichannel arrays, electrophysiological signals were individually recorded from primary mouse hippocampal neurons and recorded distinctive intracellular potential-like signals. Moreover, the transparent electrode array enabled fluorescence imaging of neuron cell bodies and neurite connections. This transparent graphene- and nanotube-based recording device is proposed to greatly increase the versatility of capabilities for investigating neuronal activity through simultaneous recording and imaging of neuron cultures.

Introduction

Vertically ordered arrays of one-dimensional (1-D) nanostructures, including nanowires, nanopillars, and nanotubes, are considered to be ideal functional components for nanoscale neural probes^{1–6}. Such 1-D nanostructures with a high aspect ratio have shown great promise for penetrating the neuron cell membrane and recording intracellular signals^{7–11}. For example, vertical silicon nanowire arrays fabricated by selective top-down etching of Si wafers have already been employed in microelectrode arrays (MEAs) to investigate the neuronal activity of individual cells to understand complex neuronal dynamics and networks^{12–15}. Recent works have demonstrated that nanoscale silicon nanowire arrays can serve as vertical structures interfacing with cell

membranes while simultaneously recording the activity of multiple cells^{12,16}. Similarly, platinum nanorods with high biocompatibility and excellent porous structures are advantageous when interfaced with cell colonies¹⁷. Other works combined field-effect transistors with kinked nanoscale silicon wire structures in arrays to non-invasively probe cell membranes that can record intracellular potentials with comparable amplitudes to those of patch clamps¹⁸. However, to record intracellular activity with minimally invasive tools, it is preferable to use sharp vertical nanostructures such as nanotubes or nanowalls. In particular, very thin nanowalls or nanotubes with thin circumferences can also provide an increased surface area that suitably interfaces the cell membrane.

Despite the significant progress in incorporating top-down processed Si-based 1D nanostructures into neural probe devices, the nontransparent nature of Si substrate-based devices makes it challenging to utilize an optical imaging technique essential for imaging the interface between the cell and the nanostructure and investigating cellular dynamics. To date, interfaces between cells and

Correspondence: Gyu-Chul Yi (gcyi@snu.ac.kr)

¹Interdisciplinary Program in Neuroscience, College of Science, Seoul National University, Seoul 08826, South Korea

²Center for Novel Epitaxial Quantum Architectures, Department of Physics and Astronomy, Seoul National University, Seoul 08826, South Korea
Full list of author information is available at the end of the article

© The Author(s) 2024



Open Access This article is licensed under a Creative Commons Attribution 4.0 International License, which permits use, sharing, adaptation, distribution and reproduction in any medium or format, as long as you give appropriate credit to the original author(s) and the source, provide a link to the Creative Commons license, and indicate if changes were made. The images or other third party material in this article are included in the article's Creative Commons license, unless indicated otherwise in a credit line to the material. If material is not included in the article's Creative Commons license and your intended use is not permitted by statutory regulation or exceeds the permitted use, you will need to obtain permission directly from the copyright holder. To view a copy of this license, visit <http://creativecommons.org/licenses/by/4.0/>.

nanostructures fabricated on opaque substrates such as silicon have been investigated using microscopy after the fixation of cells on nanostructures. These issues can be resolved if vertical 1D nanostructure arrays are prepared on transparent substrates. Here, we demonstrate the bottom-up growth of vertical ZnO nanotube arrays on graphene-based transparent substrates and the direct fabrication of nanotube electrode arrays to record individual cellular electrical signals that can be combined with optical imaging techniques.

Materials and methods

ZnO nanotube array growth on graphene layers

ZnO nanotube arrays were grown to create vertical nanostructures directly on chemical vapor deposition (CVD) graphene layers. A detailed description of the metal-organic vapor phase epitaxy (MOVPE) used to grow ZnO nanotube arrays has been previously reported. In brief, graphene layers were synthesized by CVD on Cu foil. The Cu foil was completely dissolved after being immersed in an ammonium persulfate solution, leaving only free-standing graphene layers. Then, the graphene layers were transferred onto silicon dioxide/silicon (SiO₂/Si) substrates. Next, a SiO₂ layer was precisely deposited onto the graphene layer using plasma-enhanced CVD (PECVD) and then annealed in an O₂ atmosphere for 10 min at 600 °C. The resulting hole arrays were patterned using electron beam lithography (EBL), after which the SiO₂ mask was selectively dry-etched with CF₄/Ar, followed by buffered oxide etching (BOE) to completely remove the residual oxide layer. Using catalyst-free MOVPE, ZnO nanotubes were grown on the prepared substrates. Ar was flown into the quartz reactor through the diethylzinc (DEZn) bubbler at −10 °C, while DEZn and O₂ were flown at 20 and 40 sccm, respectively. Additionally, the growth temperature and reactor pressure were both maintained at 670 °C and 300 mTorr, respectively.

Fabrication of multichannel microelectrode arrays using ZnO-based nanotubes grown on graphene

ZnO nanotube arrays were grown on a graphene/SiO₂/Si substrate with a 50 nm SiO₂ mask layer using MOVPE. To create submicron hole pattern arrays, conventional EBL was performed, followed by dry and wet etching methods. After the growth of the ZnO nanotube arrays, 1.5 μm wide electrode patterns were fabricated on the ZnO nanotube array using noncontact mask photolithography. Then, a Ti/Au (5 nm/100 nm) bilayer was deposited using a thermal evaporator to create metal contacts for the electrode patterns. The sample was rotated at a 20° angle with respect to the metal sources to conformably coat the electrodes to the ZnO nanotube. Metal lift-off was performed by immersing the substrate

in acetone to remove the remaining AZ5214e photoresist. The device was then insulated with a 3 μm-thick polyimide (PI) layer spin coated at 2000 rpm and baked for 1 min at 120 °C. Then, the perimeter of a 1 cm × 1 cm substrate was taped with Kapton tape as a frame to lift off the electrode arrays. The PI-coated ZnO nanotubes grown on graphene were separated from the underlying SiO₂ layer by mechanical lift-off. Next, the device was cured by rapid thermal annealing (RTA) in a N₂ atmosphere (3 min at 200 °C followed by 3 min at 300 °C). Next, the ZnO nanotube tips were exposed to O₂ ashing (Plasma Prep II) at 100 mTorr and 50 mA for 3 min to etch off the PI layer (1 μm). After the entire device was flipped upside down, the graphene layers at the bottom of the device were removed using O₂ ashing to electrically isolate each electrode. Then, the device was flipped back to its initial position and transferred onto a 25 mm diameter circular cover slip for transparency. To electrically connect the arrays to the recording systems, a flat-flexible cable (FFC) was attached to the devices using an anisotropic conductive film (ACF) heat bonder. To adhere a customized culture dish compatible with our device, a 3D-printed chamber was sealed onto the substrate with polydimethylsiloxane (PDMS) paste, which has adhesive properties.

Electrical characterization

The impedance of each electrode channel was characterized with a Reference 600 potentiostat (Gamry) using electrochemical impedance spectroscopy (EIS). For the corresponding three-electrode configuration measurements, the multichannel electrode array used as the working electrode was immersed in 0.01 M phosphate buffer saline (PBS), and platinum and Ag/AgCl electrodes were used as the counter and reference electrodes, respectively. Measurement signals were applied with a 5 mV AC voltage and zero DC bias for frequencies swept between 1 Hz and 10 kHz.

Cell culture

Hippocampi were isolated from the brains of 2–3 neonatal pups, dissociated in trypsin using a previously established method and seeded onto the electrode arrays¹⁹. Before plating these dissociated neuron cultures, the electrode array devices were coated with poly-D-lysine. The neuron cultures were plated with 4.2×10^5 dissociated neurons and left to grow for 10 DIV. B-26 (Gibco), Primocin (InvivoGen), and GlutaMAX (Gibco) were added to supplement Neurobasal-A medium (Gibco), which was maintained at 37 °C and 5% CO₂. For the duration of cell growth, the medium was replaced every 3–4 days. All animal experiments were conducted under methods approved by the Institutional Animal Care and Use Committee (IACUC) of Seoul National University.

Electrophysiology

Electrophysiological recordings from hippocampal neuron cultures were obtained at 10 DIV using an Intan RHS2000 controller with a ZnO nanotube array device. The controller was connected to an RHS2116 headstage adapted with an FFC connector board. Additionally, two separate Pt wires (0.3 mm diameter) were used as reference and grounding electrodes for the duration of the experiment. The data were acquired with RHX software and sampled at 30 kHz (Intan), and 0.01 Hz and 7.5 kHz filter cutoffs were used. For each device, ten individual channels were recorded through the Intan RHS2000 controller. We observed recorded signal patterns for every electrode channel to confirm that the neuron culture was being recorded. Later, the raw signals were analyzed by applying a 60 Hz notch filter and a bandwidth filter of 100 Hz using MATLAB.

Loading of calcium indicator dyes

Hippocampal neurons were prepared for calcium imaging by immersing the device in Dulbecco's modified Eagle's medium (DMEM, without Ca) (20 ml) and Dulbecco's PBS (DPBS) + CaCl (20 ml) and stored in a 37 °C incubator. Then, the original buffer was removed from the cell dish, the device was washed twice with DMEM (without Ca), and the mixture was incubated for one hour. Next, 1 vial of Fluo-4-AM (50 µg) was thawed and mixed with 6 µl of Fluo-4 in 594 µl of dimethyl sulfoxide (DMSO). Then, the dish was rinsed once with DPBS. Afterward, we mixed 5.4 ml of DPBS with 10 µM Fluo-4 solution, filled the dish with 2 ml of DPBS, and incubated the mixture for no more than one hour. Finally, the cells were rinsed twice with DPBS, and the dish was filled with 2 ml of DPBS immediately before imaging.

Fluorescence imaging

To obtain fluorescence images, an inverted microscope (Olympus IX83) with an XYZ automated stage (ASI) and an electron-multiplying charge-coupled device (EMCCD) camera (Andor) were used. A 40/0.6 numerical aperture objective (Olympus) was used to illuminate the cells under a white light emitting diode (LED) (Lumencor) for epifluorescence excitation. The same objective was used to collect fluorescence signals, which were passed through a dichroic mirror and the 49002 ET-EGFP filter set (Chroma) and finally delivered to an EMCCD camera.

Cell postfixation and SEM imaging after recordings

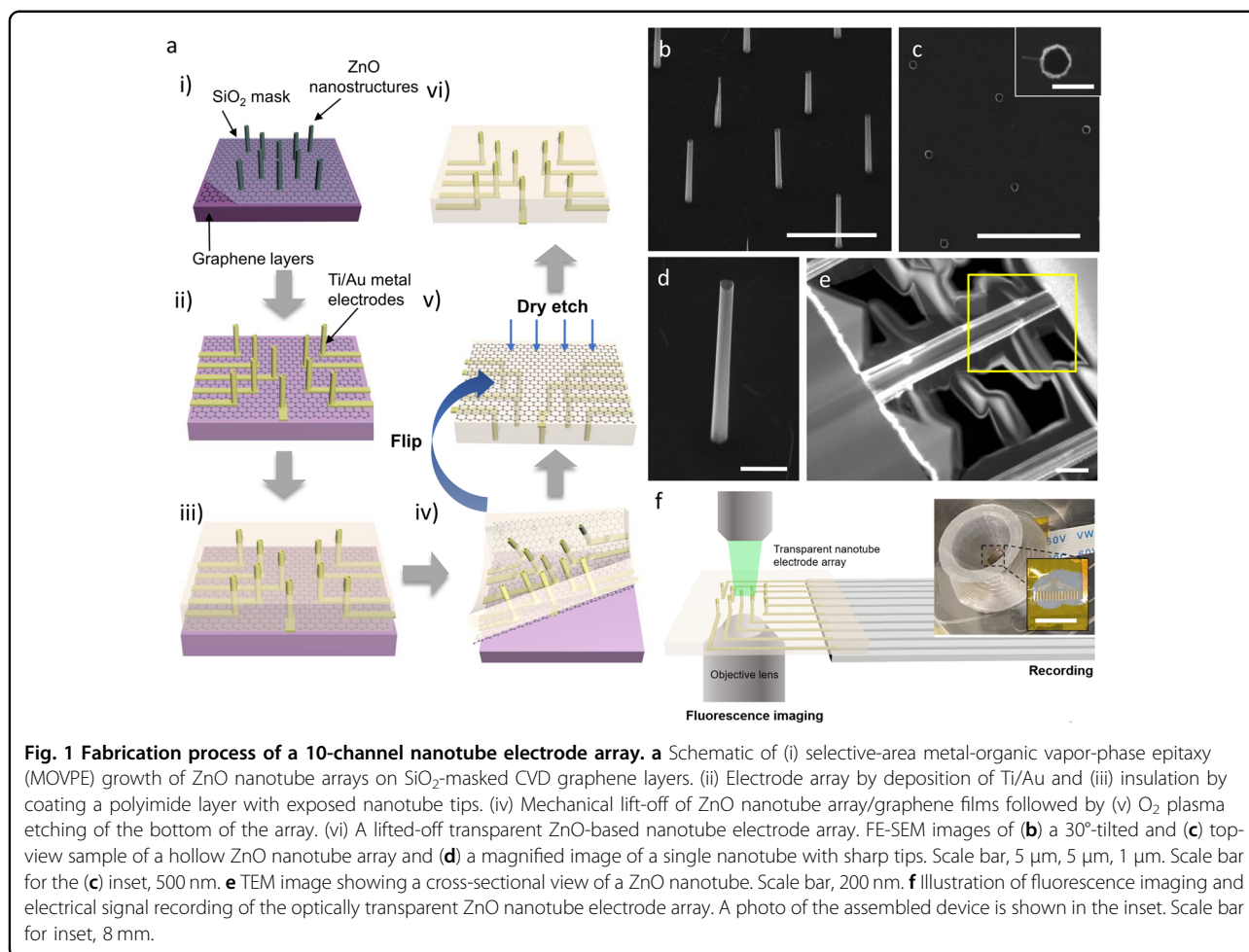
To visualize cells on the nanotube electrode, the neurons on the electrode arrays were fixed at room temperature to image the cultures that were seeded on top of the ZnO nanotube electrode arrays. First, the samples were rinsed for 1 h with 2% glutaraldehyde–paraformaldehyde in 0.1 M PBS. Another fixation buffer, 0.1 M PBS, was immediately

used to rinse the sample twice. Then, the arrays were fixed with 1% osmium tetroxide (OsO₄) dissolved in distilled water for 1 hr and rinsed three times for 5 min in distilled water. Next, the samples were dehydrated for 10 min in a series (30, 50, 70, 80, 90%) of ethanol solutions. The sample was dehydrated three times in 100% ethanol for 10 min. Finally, the sample was rinsed twice with hexamethyldisilazane (HMDS) and hydrated overnight in a vacuum chamber. After more than 12 h, a 5 nm thick Pt film was coated onto the sample using an ion coater (Leica). A field-emission scanning electron microscope (FESEM; Carl ZEISS) was used to image the fixated samples.

Results and discussion

The procedures mentioned above for fabricating transparent electrode arrays using ZnO nanotubes grown on graphene layers are illustrated in Fig. 1a. The corresponding graphene layers were synthesized on Cu foil using CVD and used as a substrate for the growth of ZnO nanotubes, which exhibited excellent transparency in the visible range^{20,21}. Vertically aligned ZnO nanotubes were selectively grown on graphene layers with a growth mask using MOVPE (Fig. 1a–i). The vapor phase epitaxial growth process enables the growth of ultrafine, crystalline nanowalls with a thickness of <30 nm that could increase the probability of natural internalization into cells^{16,22}. Scanning electron microscopy (SEM) images of a ZnO nanotube array from a 30°-tilted angle, top side, and single ZnO nanotube are shown in Fig. 1b–d, respectively. The position and dimensions of the vertical ZnO nanotube arrays were controlled by adjusting the design of the e-beam lithography pattern and the ZnO growth parameters²¹. ZnO nanotubes were selectively grown along the edges of submicron holes on the graphene layers at a growth temperature of 670 °C, as ZnO nucleation does not occur on SiO₂ at temperatures above 600 °C²³. As shown in Fig. 1b, the ZnO nanotubes used in this device were selectively grown with an average diameter of 500 nm and height of 7 µm. We confirmed the thickness of the ultrafine nanowalls was 20 ± 10 nm through a tilted SEM image of the magnified nanotubes. A cross-sectional transmission electron microscopy (TEM) image of the nanotube device array confirmed that crystalline nanotube structures formed by vapor-phase epitaxial growth (Fig. 1e). The yellow boxed region highlights the sharp upper nanowall tips of the nanotubes that interface with the cell membrane. For nanoscale neural interface devices, MOVPE-based bottom-up grown vertical nanostructures have many advantages over nanowire arrays prepared by top-down etching of Si substrates.

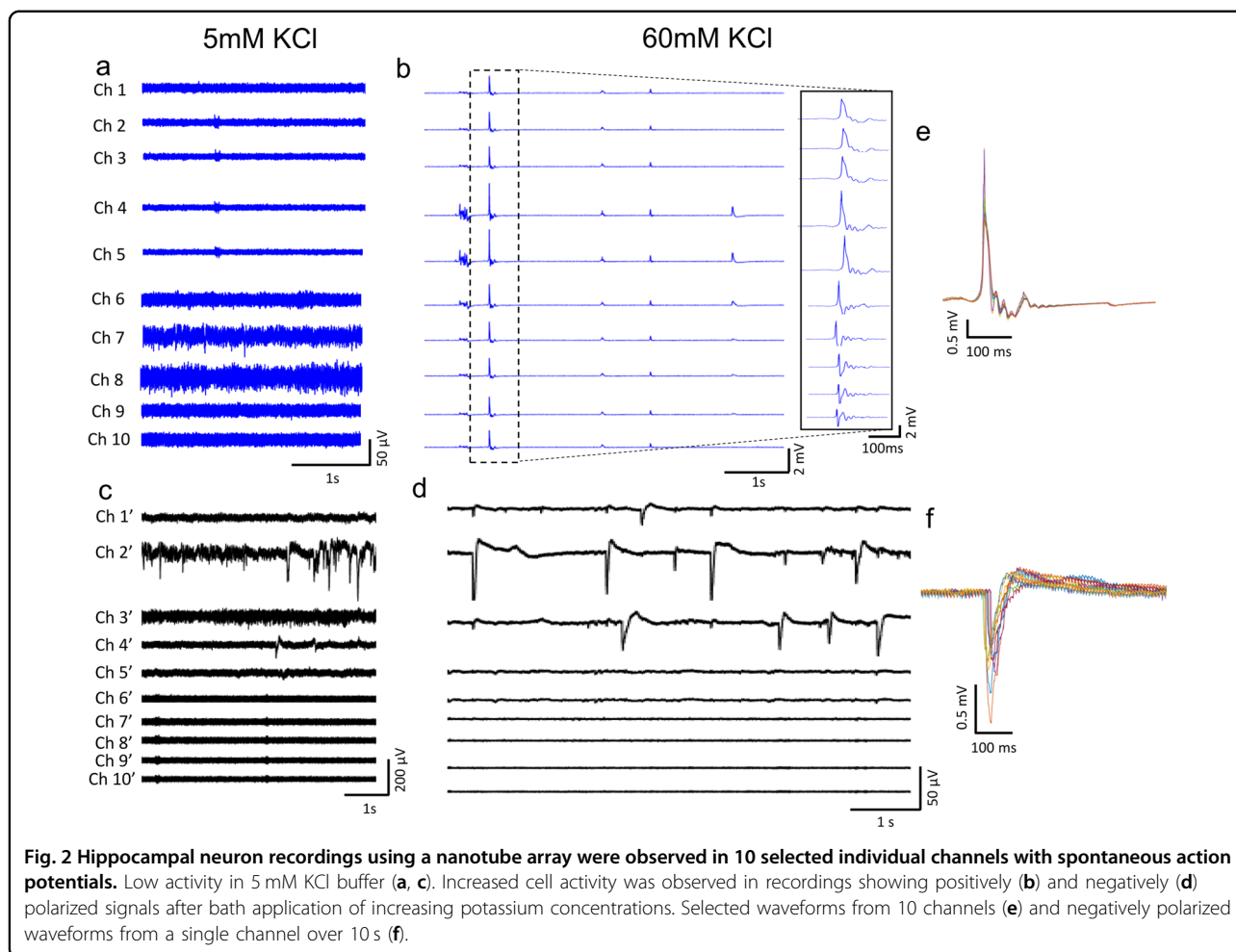
Individually addressable vertical nanotube electrode arrays were ultimately fabricated by selectively depositing metal leads on individual nanotubes within the array.



Photolithography was performed such that each nanotube was connected to an independent channel, and Ti/Au (5/100 nm) bilayers were deposited to form electrode patterns with a single nanotube throughout the array (Fig. 1a-ii). We intentionally designed electrode lines with widths less than 2 μm, which is much smaller than the typical diameters of neuron cell bodies, which are 10 μm when plated. This particular width was necessary to image the neuronal cytoplasm on top of our nanotube electrode arrays. The conformal coating of the metal bilayers was confirmed through a cross-sectional SEM image and analyzed through energy-dispersive X-ray spectroscopy (EDS) (Extended Data Fig. 1). Then, polyimide (PI) was spin-coated as an insulating layer on the entire substrate (Fig. 1a-iii), and the freestanding device was formed by lifting off the PI layer from the original substrate (Fig. 1a-iv). Here, the hybrid heterostructure of ZnO nanotube arrays grown directly on graphene layers has a weak van der Waals force with the underlying SiO₂ surface, allowing easy transfer onto foreign transparent substrates. These arrays of nanotube electrodes transferable onto transparent substrates to enable versatile

monitoring of cell dynamics based on their interactions with nanotubes as occurred over several days *in vitro*. This detachable feature is intended to complement other possible device applications, including flexible electrode arrays suitable for invasive *in vivo* studies in live animals.

The resulting freestanding nanotube array device was then connected to external electronics recording units through flat ribbon cables, transferred to a glass coverslip, and assembled with biocompatible customized culture chambers for cell culture and optical imaging. The assembled device showed an electrical impedance of less than 100 kΩ at 998.26 Hz, indicating capacitive characteristics with phases near -70°, excluding two channels with impedances of a few MΩ (Extended Data Fig. 2)²⁴. The transmission spectrum of our device fabricated on a graphene layer was 80% transparent compared to that of a conventional coverslip at a wavelength of 450 nm (Extended Data Fig. 3). As illustrated in Fig. 1f, the transparency of the ZnO/graphene hybrid heterostructure enabled fluorescent imaging and electrical recording. Compared to silicon-based nanowire arrays or electrodeposited nanostructures fabricated on opaque substrates,



graphene-based ZnO nanotube arrays can realize functional imaging that complements electrical signal recordings from the neuron cultures.

Hippocampal neurons thrived on the nanotube arrays, as observed in postfixated SEM images, which clearly showed neuronal cell bodies and neurite outgrowth (Extended Data Fig. 4). The representative top-view images obtained by SEM imaging demonstrate overlapping cells with several nanotubes and possible penetration due to the nanotube structures. Depending on the cell concentration and culture duration, selectively observed hippocampal neurons were enclosed within the nanotube arrays after 10 days in vitro (DIV). In addition, neurite outgrowth and neuronal satellite clusters were found along the structure of the nanotube array.

After the neurons were cultured on the electrode array, several devices with an array of ten channels were observed to record cellular signals that resembled intracellular and extracellular potential spikes. Multiple hippocampal in vitro cultures were recorded after the cells were seeded onto the recording arrays beginning at 7 DIV.

The resulting electrical signals of the cell–electrode interface were categorized based on amplitudes corresponding to positively or negatively depolarizing spikes, which indicated intracellular or extracellular activity. To enable a better understanding of the electrophysiological activity, both types of activity should be detectable through a single device.

Representative recordings from two separate devices both show ten channels exhibiting negative depolarization and positively depolarized spikes at 10 DIV (Fig. 2). In other words, the channels analyzed here capture intracellular and extracellular waveforms. The ten selected electrodes are separated with 10 μm pitches among the respective nanotube structures. Figure 2a and c represent cellular potential oscillations at a 5 mM KCl concentration of 4-(2-hydroxyethyl)-1-piperazineethanesulfonic acid (HEPES)-buffered saline (HBS), which was used as a baseline in comparison to heightened neuronal activity. We considered baseline stability an important factor for electrophysiological recording devices, as mentioned in previous reports²⁵. With our nanotube electrode array

device, the baseline activity did not exceed $\pm 10 \mu\text{V}$, suggesting that low noise levels are appropriate for recording neurons.

To further investigate the cellular potential in intracellular and extracellular configurations, we focused on the voltage changes in neuronal cultures before and after the addition of 60 mM KCl buffer. In this experiment, neuronal activity was triggered by the introduction of increased potassium in the extracellular medium. The concentration of potassium ions was increased to 60 mM, and the sodium ion concentration was decreased to 64 mM (usually 119 mM) to induce spiking activity. When we applied a 60 mM KCl bath, we observed distinctly depolarized neuronal membrane potentials (Fig. 2b, d) due to the high dependency of the extracellular K^+ concentration on the resting membrane potential in individual neurons. Overall, compared to baseline recordings, the frequency and amplitude of spontaneous cell activity (Fig. 2b, d) in the respective channel increased (Fig. 2a, c).

By analyzing the potential spikes, electrical waveforms resulting from voltage changes between the depolarized and resting regions were distinguishable to determine the different cell-nanotube interfaces. To validate whether the measured spikes were physiological, we modulated the chemical composition of the culture bath to increase or eliminate cellular activity. On average, the intracellular calcium concentrations increased in most cells after the application of a 60 mM KCl bath, suggesting that neuronal firing can occur more frequently in response to the 60 mM KCl bath. In particular, the potentials measured by electrodes suspected to be internalized into the cell showed positive spikes with large amplitudes of 2–4 mV, resembling the characteristic waveform of intracellular action potential activity (Fig. 2e). Based on the accumulated spikes, the time taken for depolarization to hyperpolarization was extended to 100 ms compared to conventional patch-clamp intracellular action potentials. The positive spikes detected here exhibited temporal broadening, which is consistent with prior research using intracellular nanowires to record neuronal activity^{8,12,18}. Parasitic capacitances and high electrochemical impedance between the nanostructure and the cell membrane increases the length of spikes, which are considered to be associated with the temporal broadening effect¹⁶. Additionally, the overall firing rate was low for both positive and negative depolarizations, which is expected for dissected cultures with immature neuronal networks²⁶.

We also monitored nanotube channels exhibiting extracellular spiking activity upon modulation of cellular activity. Negative potential signals with low amplitudes (0.1–0.2 mV) suggest potential changes resembling the depolarization and hyperpolarization configuration of extracellular signals (Fig. 2c). Small potential oscillations

were observed to occur before negatively depolarized cellular activity in hippocampal neuron cultures at 10 DIV (Fig. 2d). We also observed that the 60 mM KCl bath application increased the spike frequency compared to the baseline signals at 5 mM KCl, which was observed as extracellular spiking activity. Specifically, we analyzed ten spikes from a single channel induced by 60 mM KCl, which showed waveform amplitudes ranging from 0.5 mV to 1.5 mV (Fig. 2f). The observed amplitudes are slightly smaller than those in a previous report, while the period of a single spike occurrence is less than 200 ms¹². The length of a single extracellular-like spike may vary based on the location of nearby neurons relative to the nanotube recording site.

In general, we observed small oscillations after any significant spikes in any of the channels, as shown in Fig. 3. For instance, postsynaptic potential-like small potential oscillations followed by a strongly depolarized waveform for a channel resembling intracellular potential behavior were measured simultaneously with another channel showing intracellular activity spaced 10 μm apart (Fig. 3a-ii). However, we also introduced the sodium channel blocker tetrodotoxin (TTX, 1 μM) as a pharmacological intervention to suppress neuronal activities. The modulation of spiking activity depending on the introduction of either KCl or TTX determined the efficacy of the recorded electrophysiological activity (Fig. 3a-iii). Similarly, postsynaptic voltage changes were observed in all channels in the same array (Fig. 3b). Additionally, our nanotube electrode array devices detected synchronized firing activity among three or more nearby channels (Fig. 3b-i). Consistent with these findings, synchronized neuronal activity is commonly observed in neuronal cultures seeded on top of multielectrode arrays and may show an even stronger correlation among each neuron when cultured over long periods. Aside from changing the K^+ concentration during the bath application to increase neuronal activity, we did not require any other stimulation to provoke internalization of the nanotube or endocytosis of the neuron while interfacing with our device. The absence of electrical stimulation or plasmonic induction when measuring intracellular signals shows good promise for classifying and differentiating cell configurations solely by measuring cellular activities.

During continuous recording lasting more than 5 min, the maximum amplitude of potential activity increased after the bath application of 60 mM KCl and suppressed the activity of neurons after a few minutes because TTX was added to the buffer. Electrophysiological activity after the TTX application exhibited delayed signals attributed to additional drug molecules diffusing from the recorded neurons. Electrophysiological activity was eliminated after TTX treatment for all the detected channels (Fig. 3b-ii). The average activity amplitude was $\pm 100 \mu\text{V}$, which was

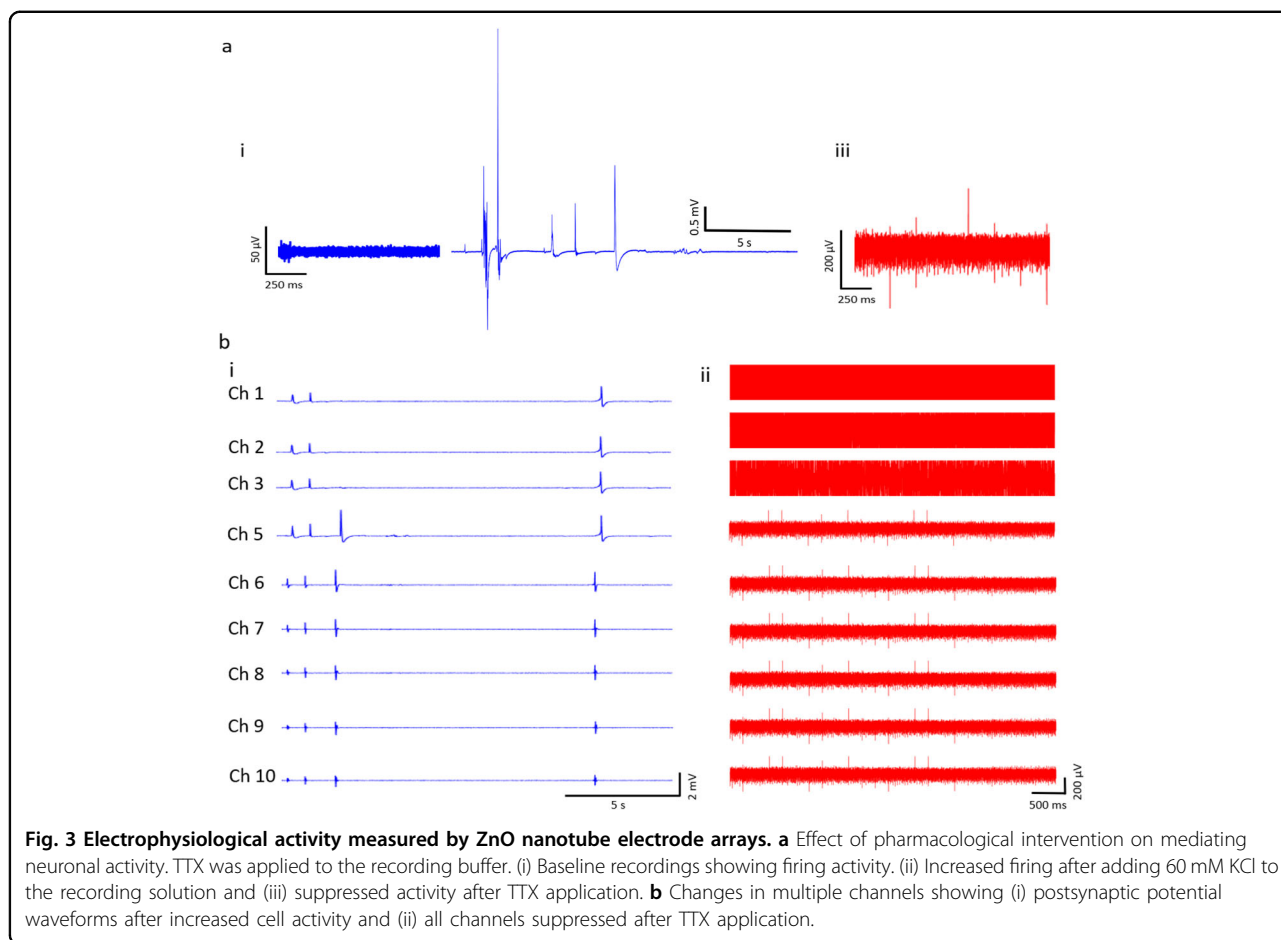


Fig. 3 Electrophysiological activity measured by ZnO nanotube electrode arrays. **a** Effect of pharmacological intervention on mediating neuronal activity. TTX was applied to the recording buffer. (i) Baseline recordings showing firing activity. (ii) Increased firing after adding 60 mM KCl to the recording solution and (iii) suppressed activity after TTX application. **b** Changes in multiple channels showing (i) postsynaptic potential waveforms after increased cell activity and (ii) all channels suppressed after TTX application.

greater than the activity before 60 mM KCl was applied, and no firing-like spikes were observed from any channel after the introduction of TTX. However, during extended durations of elevated potassium bath application, cell toxicity may increase, affecting the cell suspension and therefore leading to cell death. Additionally, we expect that the 3D-structured nanotube morphology extends upward to compromise the neuronal network, conflicting with naturally planar cell cultures. Yet, by obtaining measurements that show distinct intracellular-like and extracellular-like activities, we believe that our nanotube electrode arrays are a promising tool for mapping large-scale neuronal networks.

Finally, we performed calcium imaging in hippocampal neuron cultures using wide-field fluorescence microscopy to validate the efficiency of the imaging through transparent graphene-based arrays. Calcium imaging was conducted here because it provides single-cell spatial resolution that complements electrophysiological recordings. In this experiment, Fluo-4, a common calcium indicator dye, was applied to detect the increase in fluorescence intensity within the neuron cell body due to the rapid calcium influx associated with action potential

firing. Fluo-4 is excited at 488 nm and emits green fluorescence between 500 and 600 nm. Compared to neuron structures stained on a conventional cover slip (Fig. 4a), Fig. 4b shows a steady-state fluorescence image of the hippocampal neuron culture seeded onto the graphene-based transparent device. The selected image represents one cell body overlapping with the electrode traced through a fluorescent marker on the device. Throughout the cell culture, neuronal and dendritic connections were observed to be randomly distributed throughout the matrix near the electrode pattern marked in the white box (Fig. 4b). The transparent electrode array used here can capture neuronal cytoplasm activity in a conventional microscopic setting, thereby assisting in the observation of field recordings from large neuron populations within a single dish.

Conclusions

In conclusion, this study reports neural signals recorded by our vertical nanotube electrode array to compliment optical imaging techniques. The results are attributed to the features of our transparent and transferable graphene layers, as applied under the vertical nanotubes. Our

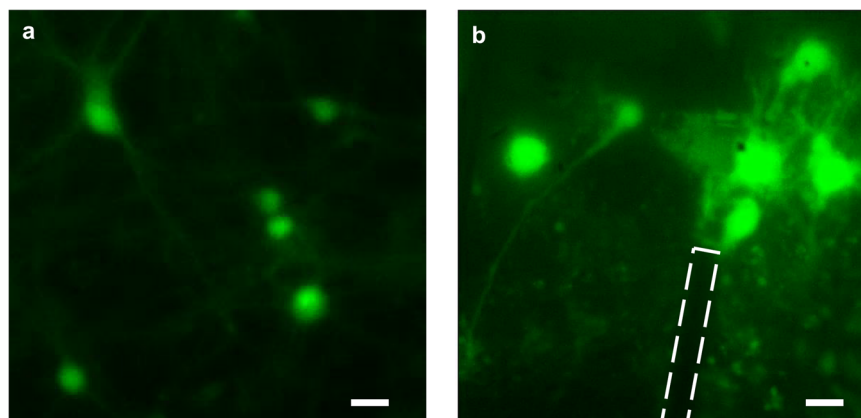


Fig. 4 Imaging of neuronal structures. Fluorescence microscopy image of neurons labeled with the Ca²⁺ indicator dye Fluo-4-AM on (a) a conventional cover slip and (b) our transparent device after electrical stimulation. The extended electrode pattern is highlighted with white patterned lines. Scale bar, 10 μ m.

resulting transparent device can be used to individually measure the electrophysiological activity of individual neurons by utilizing ZnO nanotubes with sharp nanowalls and is advantageous for furthering the investigation of neuronal networks within a single-dish culture. With additional analysis of postsynaptic potentials detectable from nearby neurons, the recording array can shed light on complex synaptic transmission plasticity and mechanisms, which are especially essential for investigating a wide range of neurological diseases. More generally, our device shows promise as an essential tool for combined electrophysiological and optical investigations of neuronal characteristics and for understanding neural circuitry.

Acknowledgements

This work was supported by the Science Research Center (SRC) for Novel Epitaxial Quantum Architectures (NRF-2021R1A5A1032996) and the Basic Science Research Program through the National Research Foundation of Korea (NRF) (2020R1A2C2007285). We also acknowledge the Brain Korea 21-Plus Program and the Institute of Applied Physics at Seoul National University for their support and availability.

Author details

¹Interdisciplinary Program in Neuroscience, College of Science, Seoul National University, Seoul 08826, South Korea. ²Center for Novel Epitaxial Quantum Architectures, Department of Physics and Astronomy, Seoul National University, Seoul 08826, South Korea. ³Integrated Electronics and Biointerfaces Laboratory, Department of Electrical and Computer Engineering, University of California San Diego, La Jolla, CA 92093, USA. ⁴Department of Electrical and Computer Engineering, University of Minnesota, Minneapolis 55455, USA. ⁵School of Biological Sciences, Seoul National University, Seoul 08826, South Korea. ⁶Institute of Molecular Biology and Genetics, Seoul National University, Seoul 08826, South Korea. ⁷Department of Biomedical Engineering, Ulsan National Institute of Science and Technology, Ulsan 44919, Republic of Korea

Author contributions

J.L.: Conceptualization, methodology, investigation, data curation, formal analysis writing-review & editing, writing—original draft. K. L.: Conceptualization, methodology. K.K.: Investigation, writing-review & editing. A.A.: Methodology, investigation. D.W.K.: Methodology, investigation, writing-

review & editing. H.A.: Methodology, investigation, writing-review & editing. Y.T.: Analysis, writing-review & editing. H.Y.P.: Writing—original draft, conceptualization, funding acquisition. G.-C.Y.: Writing—original draft, formal analysis, conceptualization, project administration, funding acquisition.

Conflict of interest

The authors declare no competing interests.

Publisher's note

Springer Nature remains neutral with regard to jurisdictional claims in published maps and institutional affiliations.

Supplementary information The online version contains supplementary material available at <https://doi.org/10.1038/s41427-024-00532-0>.

Received: 13 April 2023 Revised: 25 November 2023 Accepted: 7 December 2023

Published online: 01 March 2024

References

- Tchoe, Y. et al. Considerations and recent advances in nanoscale interfaces with neuronal and cardiac networks. *Appl. Phys. Rev.* **8**, 041317 (2021).
- Abbott, J., Ye, T., Ham, D. & Park, H. Optimizing nanoelectrode arrays for scalable intracellular electrophysiology. *Acc. Chem. Res.* **51**, 600–608 (2018).
- Zhang, A., Lee, J.-H. & Lieber, C. M. Nanowire-enabled bioelectronics. *Nano Today* **38**, 101135 (2021).
- Hong, G. & Lieber, C. M. Novel electrode technologies for neural recordings. *Nat. Rev. Neurosci.* **20**, 330–345 (2019).
- Wong-Leung, J. et al. Engineering III–V semiconductor nanowires for device applications. *Adv. Mater.* **32**, 1904359 (2020).
- No, Y.-S., Xu, L., Mankin, M. N. & Park, H.-G. Shape-controlled assembly of nanowires for photonic elements. *ACS Photonics* **3**, 2285–2290 (2016).
- Lee, K.-Y. et al. Coupling of semiconductor nanowires with neurons and their interfacial structure. *Nanoscale Res Lett.* **5**, 410–415 (2010).
- Robinson, J. T. et al. Vertical nanowire electrode arrays as a scalable platform for intracellular interfacing to neuronal circuits. *Nat. Nanotechnol.* **7**, 180–184 (2012).
- Desbiolles, B. X. E. et al. Nanovolcano microelectrode arrays: toward long-term on-demand registration of transmembrane action potentials by controlled electroporation. *Microsyst. Nanoeng.* **6**, 1–12 (2020).
- Xie, C., Lin, Z., Hanson, L., Cui, Y. & Cui, B. Intracellular recording of action potentials by nanopillar electroporation. *Nat. Nanotechnol.* **7**, 185–190 (2012).

11. Raj, V. et al. High-density individually addressable platinum nanoelectrodes for biomedical applications. *Discov. Mater.* **2**, 6 (2022).
12. Liu, R. et al. High density individually addressable nanowire arrays record intracellular activity from primary rodent and human stem cell derived neurons. *Nano Lett.* **17**, 2757–2764 (2017).
13. Elnathan, R. et al. Maximizing transfection efficiency of vertically aligned silicon nanowire arrays. *Adv. Funct. Mater.* **25**, 7215–7225 (2015).
14. Rios, G., Lubenov, E. V., Chi, D., Roukes, M. L. & Siapas, A. G. Nanofabricated neural probes for dense 3-D recordings of brain activity. *Nano Lett.* **16**, 6857–6862 (2016).
15. Lee, K.-Y. et al. Vertical nanowire probes for intracellular signaling of living cells. *Nanoscale Res Lett.* **9**, 56 (2014).
16. Liu, R. et al. Ultra-sharp nanowire arrays natively permeate, record, and stimulate intracellular activity in neuronal and cardiac networks. *Adv. Funct. Mater.* **32**, 2108378 (2022).
17. Ganji, M. et al. Selective formation of porous Pt nanorods for highly electrochemically efficient neural electrode interfaces. *Nano Lett.* **19**, 6244–6254 (2019).
18. Zhao, Y. et al. Scalable ultrasmall three-dimensional nanowire transistor probes for intracellular recording. *Nat. Nanotechnol.* **14**, 783–790 (2019).
19. Moon, H. C. & Park, H. Y. In *Methods in Enzymology* Vol. 572 (eds Filonov, G. S. & Jaffrey, S. R.) 51–64 (Elsevier, 2016).
20. Park, J. B. et al. Scalable ZnO nanotube arrays grown on CVD-graphene films. *APL Materials* **4**, 106104 (2016).
21. Kim, Y.-J. et al. Position- and morphology-controlled ZnO nanostructures grown on graphene layers. *Adv. Mater.* **24**, 5565–5569 (2012).
22. Desbiolles, B. X. E., de Coulon, E., Bertsch, A., Rohr, S. & Renaud, P. Intracellular recording of cardiomyocyte action potentials with nanopatterned volcano-shaped microelectrode arrays. *Nano Lett.* **19**, 6173–6181 (2019).
23. Tchoe, Y. et al. Individually addressable, high-density vertical nanotube Schottky diode crossbar array. *Nano Energy* **76**, 104955 (2020).
24. Park, J., Sun, F., Xie, Y., Xiong, Z. & Xu, G. Low-impedance low-artifact PEDOT: PSS-coated graphene electrodes towards high density optogenetic electrophysiology. *IEEE Electron Device Lett.* **41**, 1261–1264 (2020).
25. Yoo, J. et al. Long-term intracellular recording of optogenetically-induced electrical activities using vertical nanowire multi electrode array. *Sci. Rep.* **10**, 4279 (2020).
26. Cabrera-Garcia, D. et al. Early prediction of developing spontaneous activity in cultured neuronal networks. *Sci. Rep.* **11**, 20407 (2021).